



Research Paper

Biochar and GAC intensify anaerobic phenol degradation via distinctive adsorption and conductive properties

Qian Li^{a,b}, Xin Gao^a, Yaqian Liu^a, Gaojun Wang^{a,b}, Yu-You Li^c, Daisuke Sano^c,
Xiaochang Wang^{a,b}, Rong Chen^{a,b,*}

^a Key Lab of Environmental Engineering, Xi'an University of Architecture and Technology, No. 13 Yanta Road, Xi'an 710055, Shaanxi Province, PR China

^b Engineering Technology Research Center for Wastewater Treatment and Reuse, Xi'an University of Architecture and Technology, No. 13 Yanta Road, Xi'an 710055, Shaanxi, PR China

^c Department of Civil and Environmental Engineering, Graduate School of Engineering, Tohoku University, 6-6-06 Aza-Aoba, Aramaki, Aoba-ku, Sendai, Miyagi 980-8579, Japan



ARTICLE INFO

Editor: Prof. G. Lyberatos

Keywords:

Biochar
GAC
Phenol
Methanogenesis
Direct interspecies electron transfer

ABSTRACT

The roles of biochar and granular activated carbon (GAC) in the enhancement of anaerobic phenol degradation were characterized through batch tests conducted at different phenol concentrations, coupled with adsorption kinetics, microbial community, and in-situ electrochemical analysis. Both biochar and GAC (15 g/L) led to markedly shorter lag times (t_0) by adsorbing dissolved phenol, and faster maximum CH_4 production rate (R_{\max}) by triggering direct interspecies electron transfer (DIET) during a two-stage (adsorption then degradation) anaerobic phenol degradation. The high adsorption capacity of GAC helped achieve a shorter t_0 , but less affected R_{\max} of subsequent phenol degradation. Compared with GAC, which showed higher conductivity but no redox activity, biochar exhibited higher electron exchange capacity (6.57 $\mu\text{mol e}^-/\text{g}$). This higher electron exchange capacity stemmed from the diverse redox-active moieties, which resulted in a more efficient DIET. Meanwhile, the formation of wire-like appendages which linked the enriched DIET partners (such as *Syntrophorhabdus* and *Methanosaeta*) on biochar probably further enhanced the electron transfer. However, hydrogenotrophic methanogenesis was still the main pathway for syntrophic phenol degradation in the suspended sludge. The in-situ analysis also confirmed that biochar and GAC acted as geobatteries and geoconductors, respectively, and that the stimulation of DIET was persistent.

1. Introduction

Phenol is a toxic, intermediate chemical that is a common by-product in many industrial applications (Veeresh et al., 2005; Tian et al., 2020). Most efforts for removing phenols have been focused on their physicochemical and biological processes because of their recalcitrance and carcinogenicity (Leven et al., 2012; Aktas and Cecen, 2007). Compared with other treatment technologies, anaerobic digestion (AD) is of considerable interest for its numerous advantages, such as lower energy consumption, lower biomass yield, and its ability to promote energy recovery in the form of CH_4 (Siddique and Wahid, 2018; Mao et al., 2015). However, the high bio-toxicity of phenol to microbes and the low efficiency of hydrogen/formate interspecies electron transfer (IET) between syntrophic bacteria and methanogens limit the conversion of

phenol to CH_4 (He et al., 2019). Therefore, the addition of functional materials appears to provide a superior approach for enhancing anaerobic phenol degradation (Xu et al., 2020).

Since an alternative IET pathway—direct interspecies electron transfer (DIET)—was identified in the co-culture of *Geobacter metallireducens* and *G. sulfurreducens* (Lovley, 2017; Huang et al., 2019; Kang et al., 2019), conductive materials, such as magnetite, carbon nanotubes, granular activated carbon (GAC), and biochar have been used to enhance syntrophic methanogenesis by triggering DIET (Yuan et al., 2018; Poirier et al., 2018; Yan et al., 2018; Jiang et al., 2020). Among these materials, porous carbon—biochar and GAC are both conductive materials and ideal adsorbents (Li et al., 2019) that show a few notable advantages in anaerobic phenol degradation. First, the large surface area and high porosity of these materials can absorb dissolved

* Corresponding author at: Key Lab of Environmental Engineering, Xi'an University of Architecture and Technology, No. 13 Yanta Road, Xi'an 710055, Shaanxi Province, PR China.

E-mail address: chenrong@xauat.edu.cn (R. Chen).

<https://doi.org/10.1016/j.jhazmat.2020.124183>

Received 14 August 2020; Received in revised form 3 October 2020; Accepted 3 October 2020

Available online 8 October 2020

0304-3894/© 2020 Elsevier B.V. All rights reserved.

phenol to mitigate bio-toxicity in AD systems and promote the attachment of suspended microbes to shorten the distance between syntrophic partners (Zhao et al., 2020). Second, their conductive properties conferred by oxygen-containing moieties can improve the efficiency of syntrophic methanogenesis via DIET (Wu et al., 2020). Although one of our previous studies has confirmed that carbon-based additives promote anaerobic phenol degradation (Wang et al., 2019), the underlying mechanism of this process and its relationship to the adsorption and conductive properties of these materials require clarification.

Biochar and GAC pyrolyzed under oxygen-limited conditions below and above 1000 °C, respectively (Zhang et al., 2018b; Girods et al., 2009), results in significant differences in the adsorption and conductive properties of these materials. As mentioned above, adsorption capacity is one of the most important properties of biochar and GAC (Thang et al., 2019; Jung et al., 2001), as it determines the degree to which biotoxicity is relieved at the initial adsorption stage when anaerobic phenol degradation is enhanced and might even have an important influence on the later syntrophic methanogenesis stage. With its larger specific surface area, GAC generally shows better adsorption capacity for phenol compared with biochar (Elnaas et al., 2010; Mohammed et al., 2018); however, whether the adsorption properties of these materials are positively correlated with the efficiency of subsequent syntrophic methanogenesis and how the adsorption properties affect the kinetics of anaerobic phenol degradation remain unclear.

Because of the lower pyrolysis temperature, abundant functional groups, such as quinone/hydroquinone, can form on biochar, resulting in excellent redox activity (Klüpfel et al., 2014) but reduced conductivity (Wang et al., 2019). Compared with biochar, the graphitized structure of GAC shows high conductivity, but few oxygen-containing functional groups can survive under high temperatures. Although both redox activity and conductivity could enhance electron transfer between syntrophic partners (Wang et al., 2020; Liu et al., 2012), their contributions to DIET and the role of biochar and GAC are still unclear. In addition, the syntrophic methanogenesis of phenol occurs over an extended period compared with phenol adsorption. After biochar/GAC is enveloped by biofilm, the conductivity of this biochar/GAC-microbial polymer might change and, in turn, affect the electron transfer pathway and its efficiency. However, most studies have focused on obtaining evidence of DIET triggered by biochar/GAC via ex-situ analysis of their electrochemical properties (Yuan et al., 2018; Wang et al., 2020; Li et al., 2018), without consideration of the effects of biofilm formation. Therefore, the development of in-situ analytical methods for revealing variation in the conductive properties of biochar/GAC-microbial polymer is critical for elucidating the underlying mechanisms of enhanced anaerobic phenol degradation by biochar and GAC.

Here, batch tests were conducted with different phenol concentrations to clarify the roles of biochar and GAC in enhancing anaerobic phenol degradation. Adsorption kinetics, microbial community analysis, and in-situ electrochemical analyzes were conducted to characterize the effects of the adsorption and conductive properties of biochar and GAC on the kinetics of anaerobic phenol degradation; clarify the impact of surface properties on reducing bio-toxicity and promoting syntrophic methanogenesis, and reveal the mechanisms of electron transfer triggered by biochar and GAC.

2. Materials and methods

2.1. Biochar and GAC

Biochar used in this study was prepared at 500 °C by a muffle furnace using sawdust as a raw material as described in a previous study (Wang et al., 2020). GAC was purchased from a commercial company (Sigma-Aldrich, St. Louis, MO, USA). Both biochar and GAC were ground and sieved to diameters ranging between 0.25 and 1 mm.

2.1.1. Surface morphology and properties

The surface morphology of the biochar and GAC was analyzed by scanning electron microscopy (SEM) (JSM-6510LV, Japan). The pH value of the suspension was measured using a pH meter (PHS-3C, Dapu Instrument Co., Shanghai, China). The specific surface area was investigated by the N₂ adsorption-desorption with a V-Sorb X800 Brunauer–Emmett–Teller analyzer (Gold APP Instrument Co., Beijing, China). The elemental composition was determined by an isotope ratio mass spectrometer (IRMS, IsoPrime100, Elementar, Germany). The details for the GAC and biochar are summarized in Table S1. The organic functional groups of the biochars were determined by Fourier transform infrared spectroscopy (FT-IR, PerkinElmer, USA) with a model of attenuated total reflectance and a frequency range of 4000–900 cm. X-ray photoelectron spectroscopy (XPS) (K-Alpha, Thermo Fisher, USA) was used to study the distribution of C1s bonds distribution of GAC and biochar, and XPSPEAK was used to calibrate the C1s data. The thermogravimetry of these materials was measured by a TGA/DSC2 thermogravimetric analyzer (TGA) (Mettler-Toledo, Switzerland) following the method of Prado et al. (2019).

2.1.2. Conductive properties

A four-probe method by a powder electrical sensitivity tester (ST2722, Jingge, Suzhou, China) was used to study the electrical conductivity of the raw biochar and GAC.

The electron-accepting capacities (EAC) and electron-donating capacities (EDC) of biochar and GAC were quantified by the mediated electrochemical method with modification (Zhang et al., 2018b; Klüpfel et al., 2014). More details are provided in the Supplementary material. EAC and EDC were calculated by the following equations:

$$EAC = \frac{\int \frac{I_{EAC}}{F} dt}{m_{biochar}} \quad (1)$$

$$EDC = \frac{\int \frac{I_{EDC}}{F} dt}{m_{biochar}} \quad (2)$$

where F is the Faraday constant, m is the mass of added biochar, and I is the current with time.

The conductivity of sludge was determined using an electrochemical workstation (CHI660e, Huachen, China) according to a previous study (Yin et al., 2018).

2.1.3. Adsorption properties

Adsorption tests were conducted in 90-mL serum bottles. Biochar and GAC at dosages of 15 g/L were added into the serum bottles with an initial phenol concentration at 1000 mg/L (working volume = 50 mL, pH = 7). Next, 1 mL of supernatant was collected at different time intervals, followed by centrifugation and filtration with a 0.45 μm microfilter to determine phenol concentration. For isotherm analysis, biochar and GAC were added into the vials with different concentrations of phenol (100–1700 mg/L). After the adsorption equilibrium was reached, the supernatant was withdrawn and analyzed by the above method. All of the bottles with duplicates were incubated in a water bath shaker at 35 °C and 120 rpm. The amount of adsorbed phenol (q_e) was calculated using Eq. (3) (Dehmani et al., 2020):

$$q_e = \frac{(C_0 - C_e)V}{m} \quad (3)$$

where q_e is the adsorption capacity of biochar at equilibrium (mg/g), C_0 is the initial phenol concentration, C_e is the phenol concentration at equilibrium (mg/L), V is the volume (mL), and m is the amount of biochar (g). Kinetic and isotherm models are described in Supplementary material.

2.2. Biochar and GAC mediated anaerobic phenol degradation

2.2.1. Batch test

To elucidate the effect of the adsorption and conductive properties of biochar and GAC on anaerobic phenol degradation, batch tests were conducted. Inoculum used in this study was collected from a mesophilic UASB treating brewery wastewater. The physicochemical properties of inoculum are shown in Table S2. Twenty mL of inoculum and 5 mL of the phenol solution were added into serum bottles (120 mL); the nutrient solution (0.5 g/L NH₄Cl, 0.1 g/L MgCl₂·0.6 H₂O, 0.4 g/L K₂HPO₄, and 0.05 g/L CaCl₂·2H₂O) was replenished to obtain a 90-mL working volume with phenol concentrations of 500, 800, 1200, 1500, and 1700 mg/L. Next, 15 g/L biochar/GAC was added into each bottle; control bottles without biochar and GAC addition were also set for each phenol concentration. Moreover, blank bottles without phenol and biochar/GAC were also prepared to eliminate the influence of CH₄ generated from the inoculum when calculating the volume of CH₄ produced in the biochar-added group, GAC-added group, and control group. All of the bottles were conducted in duplicate in a mesophilic (35 °C) water bath shaker at 120 rpm. During batch tests, 1 mL of mixed sludge was taken from each bottle on the sampling days based on the degree of biogas production and stored at 4 ± 1 °C after filtration through a 0.45 μm filter.

2.2.2. Physicochemical analysis

Biogas production was measured with a glass syringe. The biogas composition (H₂, CH₄, and CO₂) was determined by a gas chromatograph (GC) (GC7900, Tianmei, China), which had a thermal conductivity detector and a molecular sieve-packed stainless-steel column (TDX-01, Shanghai, China). Phenols and volatile fatty acids (VFAs) were determined by gas chromatography (PANNO, China) with a flame ionization detector and a DB-FFAP column (φ 0.32 mm × 50 m; Agilent, USA). The benzoic acid was determined by a gas chromatography-mass spectrometer (GC-MS, Agilent, USA) with a DP5 column (30 m × 0.25 mm × 0.25 mm). Details are shown in the Supplementary material.

The CH₄ production of each group was fitted using the following modified Gompertz equation (Li et al., 2020):

$$P = P_0 \cdot \exp \left\{ - \exp \left[\frac{R_{max} \cdot e}{P_0} \cdot (t_0 - t) + 1 \right] \right\} \quad (4)$$

where P refers to methane production (mL), P_0 is the CH₄ production potential (mL), R_{max} is the maximum CH₄ production rate (mL/d), t_0 is the lag time (days), and e is a constant. The Origin software (Origin Lab 2018 Corporation, USA) was used to analyze the significance of differences in the data by one-way analysis of variance (ANOVA).

2.3. Characteristics of enriched microbes by biochar and GAC

2.3.1. Morphology

One g of biochar and GAC was taken from bottles at a phenol concentration of 800 mg/L after batch tests of anaerobic phenol degradation were complete. The morphology of the enriched microbes on biochar and GAC was analyzed by SEM (JSM-6510LV, Japan).

2.3.2. Microbial communities

Five samples were taken from the biochar-added group (attached biofilm on biochar and the suspended sludge with biochar removal), GAC-added group (attached biofilm on GAC and the suspended sludge with GAC removal), and control group at a phenol concentration of 800 mg/L. DNA was extracted from the five samples using the E.Z.N.A.® soil DNA Kit (Omega Bio-tek, Norcross, GA, USA) per the manufacturer's instructions. The extracted DNA was then purified by a 1% agarose gel, and the DNA concentration was determined by a NanoDrop 2000 UV-Vis spectrophotometer (Thermo Scientific, Wilmington, DE, USA).

High-throughput sequencing (HTS) targeting 16S rRNA was used to analyze the microbial communities. The hypervariable region V4 of the bacterial 16S rRNA gene was amplified with the primer pairs 515F (5'-GTGCCAGCMGCCGCGTAA-3') and 806R (5'-GGAC-TACHVGGGTWTCTAAT-3') by anABI GeneAmp® 9700 PCR thermocycler (ABI, CA, USA). For the archaea, the primers 340F (5'-CCCTAYGGGGYGCASCAG-3') and 1000R (5'-GGCCATGCACYWYCCTCTC-3') were used. PCR reactions were conducted in triplicate with the mixtures, which contained 5× TransStartFastPfu buffer 4 μL, 2.5 mM dNTPs 2 μL, forward primer (5 μM) 0.8 μL, reverse primer (5 μM) 0.8 μL, TransStartFastPfu DNA Polymerase 0.4 μL, template DNA 10 ng, and ddH₂O up to 20 μL. The PCR products were extracted using a 2% agarose gel and purified by the AxyPrep DNA Gel Extraction Kit (Axygen Biosciences, Union City, CA, USA) per the manufacturer's instructions. HTS was performed by a commercial company (Majorbio Co., Ltd., Shanghai, China) using the Illumina Miseq sequencing system (Illumina, USA).

2.3.3. Electrochemical properties of biochar/GAC-microbial polymers

To characterize the effects of attached microbes on the electrochemical properties of biochar and GAC, the electrochemical responses of biochar/GAC-microbial polymers were investigated by in-situ cyclic voltammetry (CV) in an H-type cell with modification (Fig. S1) (Yan et al., 2018). The same mass of GAC and biochar (1.5 g) was dropped casted on the carbon felt (1 cm²) by mixing with 40 μL of nafion, which was externally connected to working electrodes in an anodic chamber [versus Ag/AgCl/Cl (sat.)]. This chamber contained 100 mL of fresh-water medium with 100 mg/L of phenol and 20 mL of the acclimatized seed sludge. A graphite plate (3.0 cm × 1.5 cm) was used as a counter electrode. The CV of the three electrodes was sequentially conducted at 10 mV/s (−1.2 to 1.2 V) with $t = 0$. After the biofilm attached on the biochar/GAC (i.e., the biochar/GAC-microbial polymer), the electrochemical properties of the polymers were analyzed under the same voltage versus Ag/AgCl.

The value of the electron transfer coefficient (k_{app}) was calculated using Eq. (5) (Yuan et al., 2011):

$$E_p = E^0 - \left(\frac{RT}{(1-\alpha)nF} \right) \ln \frac{(1-\alpha)nFv}{RTk_{app}} \quad (5)$$

where E_p is the anodic peak potential; v is the sweep rate; k_{app} is the electron transfer coefficient; and R , T , and F are constants ($R = 8.314 \text{ J mol}^{-1} \text{ K}^{-1}$, $T = 298 \text{ K}$, and $F = 96,483 \text{ C mol}^{-1}$). The $(1-\alpha)nF$ quantity is calculated from the slope of the linear portion of the $(E_p - E^0)$ versus $\ln(v)$ curves.

3. Results and discussion

3.1. Different phenol degradation kinetics derived from biochar and GAC addition

The accumulated CH₄ production data at phenol concentrations ranging from 500 to 1700 mg/L are shown in Fig. 1a–c, and kinetics parameters obtained by Gompertz model fitting are listed in Table 1. In the control group, the bio-toxicity of dissolved phenol inhibited CH₄ production; thus, lag time (t_0) was the longest (15.8 d) among treatments, even at the lowest phenol concentration of 500 mg/L, and completely stagnated at phenol concentrations above 800 mg/L. However, both biochar and GAC could promote CH₄ production at even the highest phenol concentration (1700 mg/L), although the adsorption capacity (expressed as adsorbable phenol at a dosage of 15 g/L) of biochar (814.5 mg/L) was significantly lower than that of GAC (1523 mg/L). The decrease in phenol concentration in the absence of CH₄ production in the control group (at concentrations of 1200, 1500, and 1700 mg/L) indicated that approximately 12% phenol could be adsorbed by the suspended microbes (abiotic adsorption could be

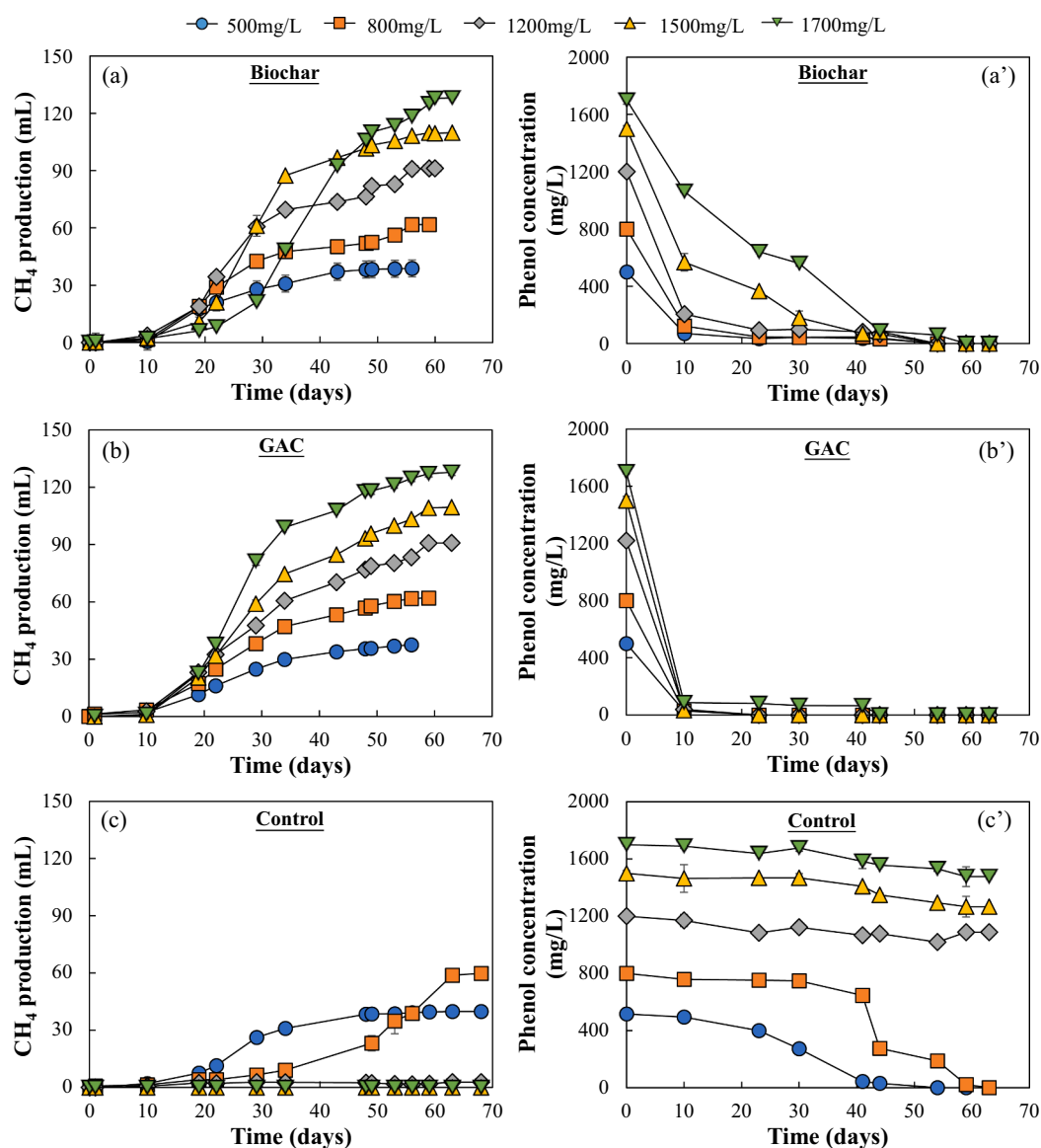


Fig. 1. CH₄ production and phenol concentration variation for biochar (a) (a'), granular activated carbon (GAC) (b) (b'), and control groups (c) (c') at 500, 800, 1200, 1500, and 1700 mg of phenol/L.

neglected) (Fig. 1c). Thus, GAC completely adsorbed phenol before it was converted to CH₄, even at a concentration of 1700 mg/L, which was slightly higher than its adsorption capacity (Fig. 1b'). Because of the lower adsorption capacity of biochar, residual dissolved phenol was observed when the phenol concentration was greater than 1200 mg/L (Fig. 1a'). The incomplete adsorption might be the main factor underlying the longer lag time in the biochar-added group compared with that in the GAC-added group. Nevertheless, COD mass balance confirmed that more than 95% of phenol could be converted to CH₄ once microbes recovered from inhibition, indicating an efficient phenol degradation was achieved in this two-stage process.

When the phenol concentration was lower than the adsorption capacity, the t_0 of CH₄ production in both the biochar and GAC-added groups was maintained for approximately 10 days, as the dissolved phenol was almost completely adsorbed by biochar/GAC, thus reducing bio-toxicity (Fig. 2a) (Poirier et al., 2016). When the phenol concentration was greater than the adsorption capacity, t_0 was prolonged almost linearly with a similar slope. Thus, t_0 might only be affected by the adsorption capacity of carbon additives, regardless as to whether biochar or GAC was added.

The maximum CH₄ production rate (R_{max}) increased linearly with phenol concentration in both the biochar ($R^2 = 0.98$) and GAC-added group ($R^2 = 0.99$) (Fig. 2b). Nevertheless, the R_{max} in the biochar-added group was 14.8–81.9% higher than that in the GAC-added group at the same phenol concentration, although a decrease in R_{max} was observed at the maximum phenol concentration of 1700 mg/L. By contrast, the increase of R_{max} in the biochar-added group was more rapid, which was 1.83 times that of the GAC group. In addition, the relative content of benzoic acid (Fig. S2) implied that biochar was superior for overcoming the thermodynamic barriers of benzoic acid oxidation (Eq. (6)), thus enhancing the methanogenesis of adsorbed phenol. The excellent capacity of biochar to promote methanogenesis might be related to its distinct conductive properties.

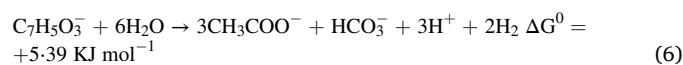


Table 1
Kinetic parameters of CH₄ production in the biochar-added group, granular activated carbon (GAC)-added group, and control group (CT) obtained by Gompertz equation fitting.

Parameters	500 mg/L			800 mg/L			1200 mg/L			1500 mg/L			1700 mg/L		
	biochar	GAC	CT	biochar	GAC	CT	biochar	GAC	CT	biochar	GAC	CT	biochar	GAC	CT
t_0 (days)	9.1 ± 1.7	10.5 ± 0.5	12.7 ± 0.6	9.5 ± 1.8	10.5 ± 0.6	20.1 ± 2.2	15.2 ± 1.6	10.9 ± 1.3	-	18.2 ± 0.5	12.6 ± 1.1	-	24.6 ± 0.7	15.5 ± 0.8	-
R_{max} (mL/d)	1.6 ± 0.2	1.4 ± 0.1	1.1 ± 0.1	2.2 ± 0.8	2.1 ± 0.1	1.42 ± 0.3	5.0 ± 0.5	2.8 ± 0.2	-	5.9 ± 0.3	3.7 ± 0.2	-	5.2 ± 0.3	4.3 ± 0.4	-
R^2	0.98	0.99	0.99	0.98	0.99	0.96	0.98	0.99	-	0.99	0.98	-	0.99	0.99	-

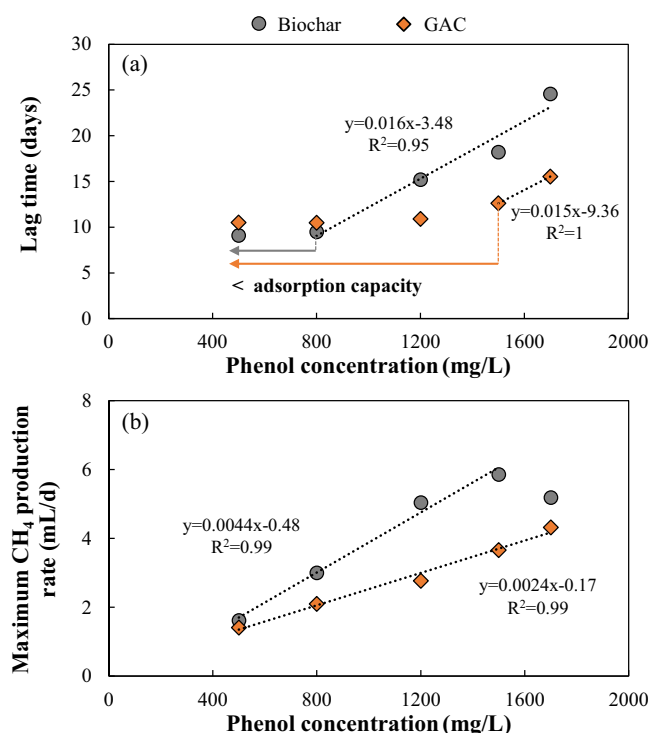


Fig. 2. The (a) lag time (t_0), (b) maximum rate of CH₄ production (R_{max}) at different phenol concentrations.

3.2. Distinct surface structures confer different adsorption and conductive properties

3.2.1. Adsorption properties

SEM showed that biochar had an inclined tube-like shape and well-arranged pores with cylindrical morphologies (diameters of 6–7.2 μm) (Fig. S3a) that originated from the vascular cells of plant tissue (Keilweit et al., 2010). However, GAC exhibited a more rugged morphology with larger and more heterogeneous holes (Fig. S3b) and larger specific surface area (762.5 > 83.6 m^2/g), which likely explains why GAC is a better adsorbent compared with biochar. Adsorption kinetics and isotherm analysis (Supplementary material) indicated that chemisorption controlled the adsorption process of phenol by these two materials because of the higher R^2 for the pseudo-second-order model (Mohammed et al., 2018). The adsorption equilibrium concentration of GAC was 33.54 mg/g, which was 1.75 times that of biochar. Moreover, the maximum phenol adsorption capacities were 54.3 and 101.53 mg/g for biochar and GAC, respectively. The high adsorption capacity of GAC was beneficial for mitigating the sudden increase in bio-toxicity caused by dissolved phenol. Thus, the t_0 of CH₄ production could be maintained at 15.5 d, even under a phenol concentration as high as 1700 mg/L, which was significantly lower than the t_0 for the biochar-added group (24.6 d). Although the morphology and specific surface area were remarkably different, t_0 was only determined by the difference in phenol concentration and adsorption capacity of biochar/GAC.

3.2.2. Conductive properties

Higher diversities of organic functional groups, $-(\text{CH}_2)-$, aliphatic C–O, C=C, and other aromatic structures were detected on biochar relative to GAC (Fig. 3a) (Yu et al., 2015; Kan et al., 2016). Furthermore, redox (hydro) quinone moieties (vibration at 1570/cm) were richer on biochar than on GAC (Yu et al., 2015; Saquing et al., 2016), which was consistent with the results of the TGA and XPS analyzes (Fig. 3b–d). A remarkable C=O bond at 286.4 eV and 287.4 eV and the hump at 600–800 $^\circ\text{C}$ were assigned to redox quinone/carbonyl moieties (Prado

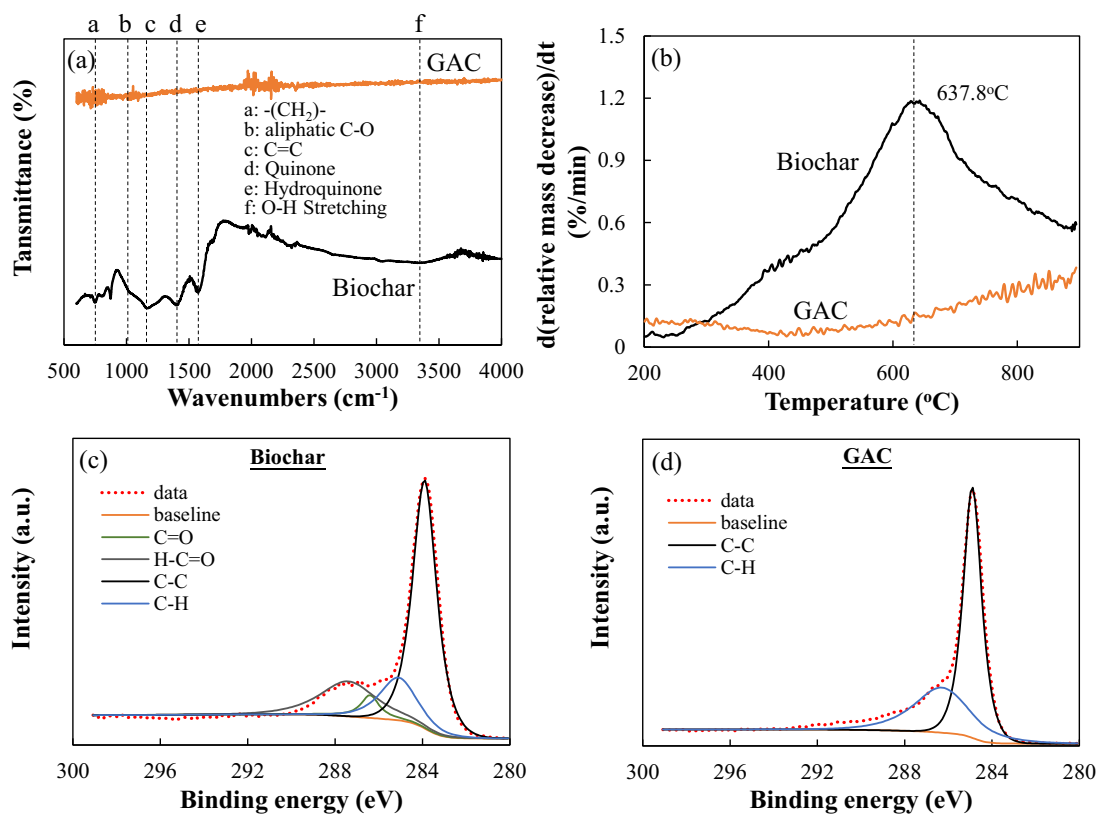


Fig. 3. Fourier transform infrared spectroscopy (FT-IR) (a) and thermogravimetric Analysis (TGA) (b) and X-ray photoelectron spectroscopy (XPS) analysis (c) (d) of biochar and granular activated carbon (GAC).

et al., 2019), which could be responsible for making biochar redox active (Yuan et al., 2018). However, GAC was more conductive than biochar, as the C1s spectra of GAC showed a higher abundance of the C-H and C-C bands than biochar at 284.8 eV and 250.3 eV, respectively.

The distinct surface functional groups of biochar and GAC were responsible for the significantly different conductive properties of these two carbon materials. The EDC and EAC of biochar were 0.38 and 6.19 $\mu\text{mol e}^-/\text{g}$ respectively, indicating that biochar was a redox mediator that tended to accept electrons in redox reactions, which is consistent with the findings of Klüpfel et al. (Fig. 4a) (Klüpfel et al., 2014). Interestingly, although GAC was not capable of redox-based electron exchange because of the loss of quinone-like oxygen-

containing moieties caused by the higher temperature of pyrolysis and the formation of a condensed graphitic sheet, the conductivity of the mixed sludge of the GAC-added group was $67.45 \pm 1.30 \mu\text{S}/\text{cm}$ (Fig. 4b). The capacity for conductivity enhancement was as high as 4.16 $\mu\text{S}/\text{cm}/\text{g}$, which was 8.82 times higher than that for biochar (0.47 $\mu\text{S}/\text{cm}/\text{g}$), suggesting that GAC could act as a geoconductor and increase the capacity for electron exchange (Zhao et al., 2016). The markedly higher R_{max} in the biochar-added group indicated that the redox-based electron exchange capacity likely played a more important role in promoting DIET than conductivity.

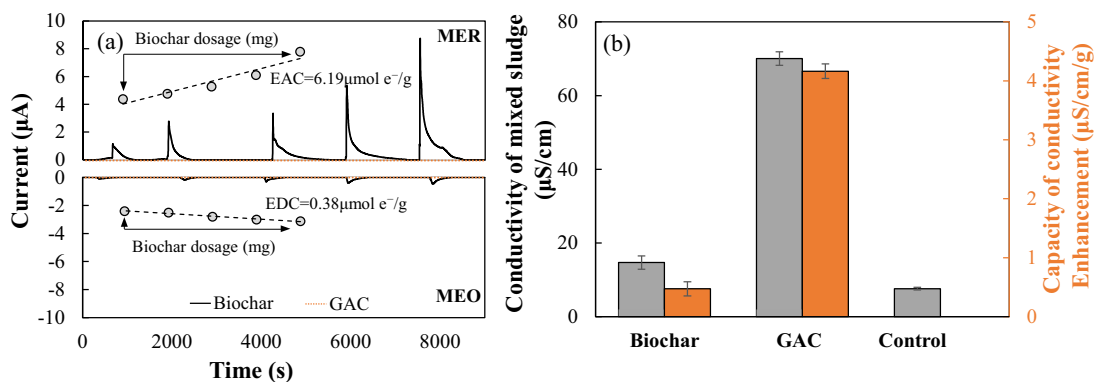


Fig. 4. (a) Reductive and oxidative current responses to increasing amount of biochar (black curve) and GAC (orange curve) analyzed by mediated electrochemical reduction (MER) and mediated electrochemical oxidation (MEO). The current increased almost linearly with biochar dosage (insert), but no response with GAC dosage. The slopes of linear regression lines of current versus biochar dosage correspond to the electron accepting capacity (EAC) and electron donating capacity (EDC). (b) electrical conductivity analysis for the sludge samples. The gray bars were the conductivity of mixed sludge in biochar-added group, GAC-added group and control group, orange bars were the enhanced conductivity of mixed sludge introduced by biochar and GAC per unit mass. (For interpretation of the references to color in this figure legend, the reader is referred to the web version of this article.)

3.3. Enrichment of functional microbes induced by biochar and GAC

3.3.1. Succession of microbial communities

Bacteria and archaea with relative abundances > 1% were analyzed. *Syntrophorhabdus*, which can oxidize phenol to acetate via syntrophic associations with hydrogenotrophic methanogens (Qiu et al., 2008), only accounted for 2.06% of the total bacteria in the control group but was the most abundant bacterial genus in the attached biofilm of the biochar-added group and GAC-added group with relative abundances of 28.6% and 23.3%, respectively (Fig. 5a). The high abundance of *Syntrophorhabdus* on biochar and GAC might play an important role in the enhancement of syntrophic phenol degradation. *Syntrophobacter* and no rank_f_Syntrophaceae, two common syntrophic VFA-oxidizing bacteria (Zhang et al., 2018a; Gray et al., 2011), were the dominant genera in the suspended sludge (with biochar/GAC removal) in both the biochar (15.6% and 14.0%) and GAC-added (15.3% and 8.65%) groups, but their relative abundances in the attached biofilm of the biochar-added, GAC-added, and control groups were lower. The enrichment of *Syntrophobacter* and no rank_f_Syntrophaceae in the suspended sludge likely stemmed from the alleviation of bio-toxicity as phenol was adsorbed by biochar and GAC. In addition, *Thermovirga*, which could contribute to the syntrophic degradation of phenol, was highly enriched in the suspended sludge of the GAC-added group with a relative abundance of 10.7%, which was significantly higher than that observed in the biochar and control groups. The enrichment of *Thermovirga* in the suspended sludge of GAC might mitigate the bio-toxicity shock (Dahle and Birke-land, 2006; Sun et al., 2020), permitting the production of CH₄ to begin early in the digestion process, even under high phenol concentrations.

Methanosaeta (*Methanotherix*) and *Methanobacterium* were the dominant archaeal genera (Fig. 5b). The relative abundance of *Methanosaeta* on biochar and GAC was 51.6% and 55.3%, respectively, which was 75% and 63% higher relative to the control group. *Methanosaeta* could not only produce CH₄ via the acetoclastic pathway but also DIET by bicarbonate reduction (Liu et al., 2012). Thus, the highly abundant *Methanosaeta* in the attached biofilm on biochar and GAC might stimulate highly efficient DIET between syntrophic partners. The hydrogenotrophic methanogen *Methanobacterium* was the most dominant genus in the control group (65.2%); the relative abundances of hydrogenotrophic

methanogens were also higher than the acetoclastic methanogens in the suspended sludge of the biochar-added and GAC-added groups. We speculate that IET via hydrogenotrophic methanogenesis was still the main pathway for syntrophic phenol degradation in the suspended sludge and that DIET might occur between syntrophic microbes enriched on biochar and GAC because of their conductive properties.

3.3.2. Morphology of enriched microbes

Although the dominant bacteria and archaea, such as *Syntrophorhabdus* and *Methanosaeta*, enriched on biochar and GAC were similar, the morphology of microbial clusters were significantly different, as shown in Fig. 6. Microbes tended to attach to the surface of GAC, whereas they tended to occupy the internal pores of biochar. In addition, wire-like appendages that linked microbes as bridges were observed on biochar, which were probably stimulated by the distinct properties of biochar, especially the highly redox-based electron exchange capacity. It could be speculated that the wire-like appendages might link the syntrophic partners as electron channels during DIET, thus, more positively promoting the syntrophic phenol degradation.

3.4. Persistent stimulation of biochar/GAC-microbial polymer

An in-situ CV method was used to clarify variation in the electrochemical properties of biochar and GAC. The redox peaks found on the CV curve of biochar confirmed its redox-based electron exchange capacity, which tended to be more reversible after the biofilm attached to biochar in the anaerobic phenol degradation system (Fig. 7a). In contrast, a smooth CV curve for GAC could be observed (Fig. 7b). This curve for the GAC-microbial polymer became increasingly steep, generating a current that was four times higher than that of biochar (day 8). The similar electrochemical properties before and after biofilm attachment (formation of biochar/GAC-microbial polymer) indicated that the promotion of syntrophic phenol degradation by biochar and GAC was temporally persistent.

To clarify the redox properties of biochar/GAC-microbial polymers, the CV curves were obtained under scan rates of 10–30 mV/s (Fig. 7c and d). The biochar-microbial polymer showed clear redox peaks (0.17, -0.18, and -0.77 V, versus Ag/AgCl) under each scan rate, but the

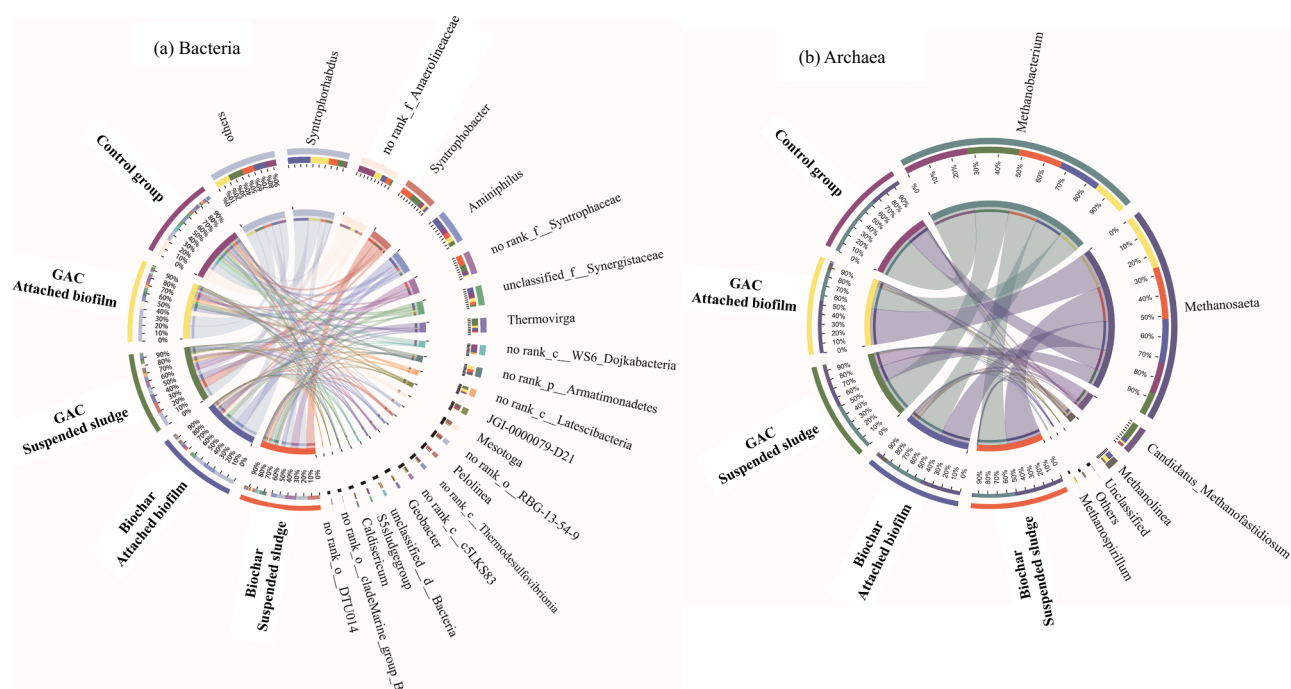


Fig. 5. Community structure of (a) bacteria and (b) archaea at the genus level.

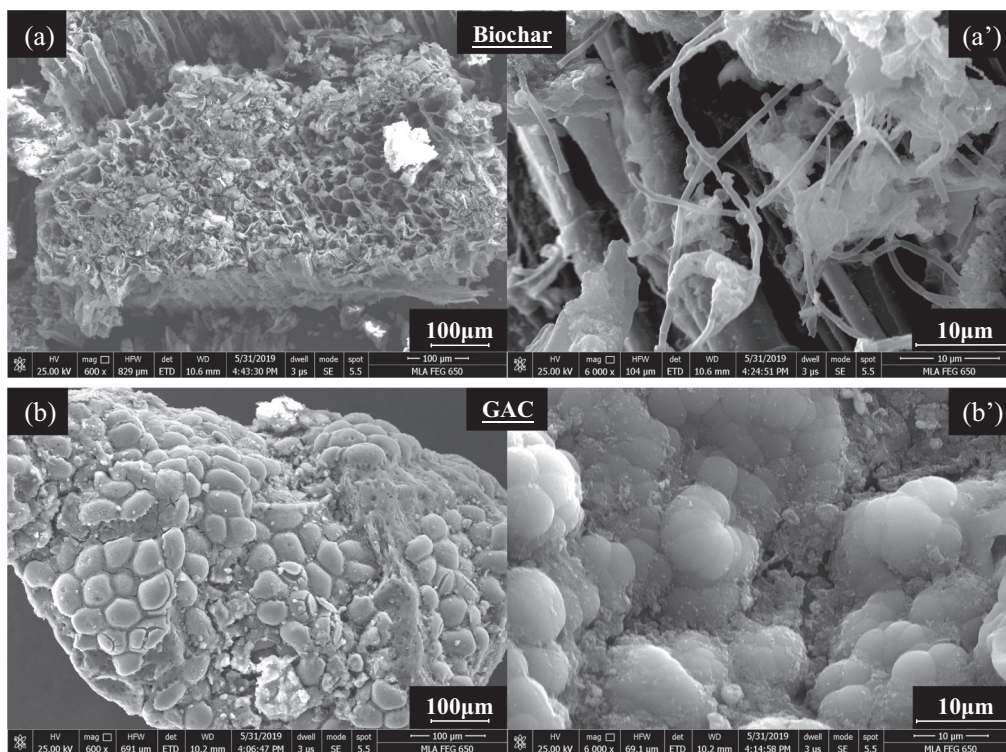


Fig. 6. Scanning electron microscopy (SEM) micrographs of biochar (a, 100 μm) (a', 10 μm) and granular activated carbon (GAC, b, 100 μm) (b', 10 μm) after completion of the batch tests.

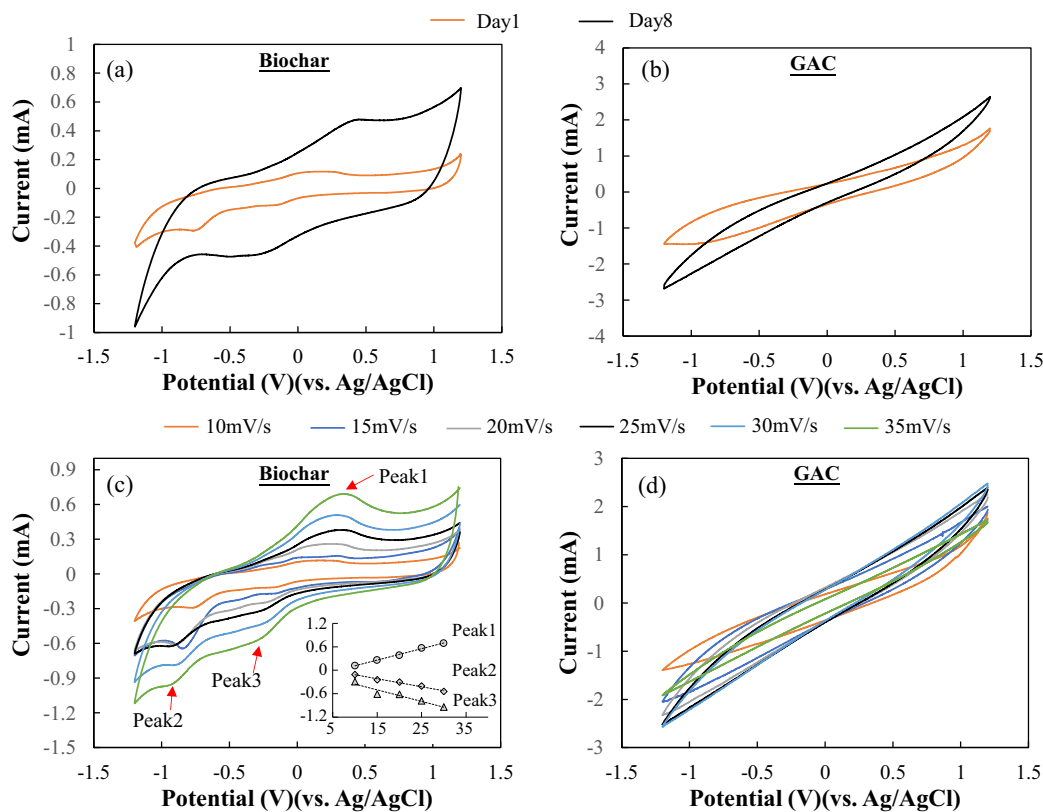


Fig. 7. The in-situ analysis of the microbial response to biochar (a) and granular activated carbon (GAC)-modified (b) anode just after inoculation ($t = 1$) and after polarization at 0.2 V (vs. Ag/AgCl/Cl (sat.)) for 7 days to promote biofilm growth; scan rate = 10 mV/s; freshwater medium with 1 mM phenol. Cyclic voltammetry of biochar (c)/GAC (d)-microbial polymer measured at different scan rates (10–30 mV/s). The insert in (a) indicates the linear analysis of the scan rate and the current at the different peaks.

GAC-microbial polymer only showed a smooth curve with an intensified current response. Although the relationship between the interface redox reaction and the syntrophic phenol was difficult to quantify, the linearly increasing peak currents of biochar as scan rates increased suggested that these redox reactions for electron transfer showed typical forms of kinetic control (Yuan et al., 2011; Laviron, 1979). The value of the electron transfer coefficient (k_{app}) was 0.0856 ± 0.003 , which was comparable to that of ferrocene during AD (Yin et al., 2018). The distinct k_{app} suggested that redox-based extracellular electron transfer occurred on biochar instead of GAC. Specifically, the CV curve obtained at a rate of 10 mV/s revealed an obvious redox peak centered at the potential of -0.139 V versus Ag/AgCl for biochar. This potential was more positive than the midpoint potentials of general cytochromes from the biomass, which likely involved microbial electron transfer induced by biochar-microbial polymer (Kracke et al., 2015).

4. Conclusions

Both biochar and GAC significantly promoted CH₄ production during anaerobic phenol degradation via a two-stage (adsorption, then degradation) process. Although the adsorption capacity of GAC was higher than that of biochar, which remarkably mitigated bio-toxicity induced by dissolved phenol, the CH₄ production rate was determined mainly by the conductive properties. GAC exhibited high conductivity but was not redox-active. By contrast, biochar showed a higher electron exchange capacity because of the diverse redox-active moieties, which could act as electron shuttles for electron exchange between enriched syntrophic partners via wire-like appendages formed on biochar, thus triggering a more efficient DIET. Although the DIET mainly occurred on the surface of biochar and GAC, the stimulation of DIET was persistent, even after biochar and GAC had been enveloped by biofilm.

Notes

The authors declare no competing financial interests.

CRedit authorship contribution statement

Qian Li: Conceptualization, Investigation, Writing - original draft, Funding acquisition. **Xin Gao:** Methodology, Investigation, Data curation. **Yaqian Liu:** Formal analysis, Visualization. **Gaojun Wang:** Methodology, Formal analysis. **Yu-You Li:** Writing - review & editing. **Daisuke Sano:** Writing - review & editing. **Xiaochang Wang:** Resources, Writing - review & editing. **Rong Chen:** Writing - review & editing, Project administration, Supervision, Funding acquisition.

Declaration of Competing Interest

The authors declare that they have no known competing financial interests or personal relationships that could have appeared to influence the work reported in this paper.

Acknowledgments

This work was supported by the National Natural Science Foundation of China (Grant Nos. 51978560, 52070148), the National Key Research and Development Program of China (No. 2017YFE0127300), and the Shaanxi Provincial Program for Innovative Research Team (No. 2019TD-025).

Appendix A. Supplementary material

Physicochemical properties of biochars (Table S1), characteristics of the seed sludge (Table S2), the adsorption capacity of phenol by adsorption kinetics and isotherm analysis, parameters of phenol adsorption kinetics (Table S3) and adsorption isotherms (Table S4),

analysis of benzoic acid, electron exchange capacity of biochar, characterization of the biochar/GAC-microbial polymer, H-type cell with modification (Fig. S1), the relative content of benzoic acid determined by GC-MS at 1 d and 9 d in the biochar and GAC-added groups (Fig. S2), SEM figures of biochar (a) and GAC (b) (Fig. S3).

Supplementary data associated with this article can be found in the online version at doi:10.1016/j.jhazmat.2020.124183.

References

- Aktas, O., Cecen, F., 2007. Adsorption reversibility and bioregeneration of activated carbon in the treatment of phenol. *Water Sci. Technol.* 55, 237–244.
- Dahle, H., Birkeland, N.K., 2006. *Thermovirga lienii* gen. nov., sp. nov., a novel moderately thermophilic, anaerobic, amino-acid-degrading bacterium isolated from a North Sea oil well. *Int. J. Syst. Evol. Microbiol.* 56, 1539–1545.
- Dehmani, Y., Sellaoui, L., Alghamdi, Y., Lainé, J., Badawi, M., Amhoud, A., Bonilla-Petriciolet, A., Lamhasni, T., Abouarnadasse, S., 2020. Kinetic, thermodynamic and mechanism study of the adsorption of phenol on Moroccan clay. *J. Mol. Liq.* 312, 113383.
- Elnaas, M.H., Alzuhair, S., Alhajia, M.A., 2010. Removal of phenol from petroleum refinery wastewater through adsorption on date-pit activated carbon. *Chem. Eng. J.* 162, 997–1005.
- Girods, P., Dufour, A., Fierro, V., Rogaume, Y., Rogaume, C., Zoulalian, A., Celzard, A., 2009. Activated carbons prepared from wood particleboard wastes: characterisation and phenol adsorption capacities. *J. Hazard. Mater.* 166, 491–501.
- Gray, N.D., Sherry, A., Grant, R.J., Rowan, A., Head, I.M., 2011. The quantitative significance of Syntrophaceae and syntrophic partnerships in methanogenic degradation of crude oil alkanes. *Environ. Microbiol.* 13, 2957–2975.
- He, C., Lin, W., Zheng, X., Wang, C., Hu, Z., Wang, W., 2019. Synergistic effect of magnetite and zero-valent iron on anaerobic degradation and methanogenesis of phenol. *Bioresour. Technol.* 291, 121874.
- Huang, L., Liu, X., Tang, J., Yu, L., Zhou, S., 2019. Electrochemical evidence for direct interspecies electron transfer between *Geobacter sulfurreducens* and *Prosthecochloris aestuarii*. *Bioelectrochemistry* 127, 21–25.
- Jiang, Q., Chen, Y., Yu, S., Zhu, R., Zhong, C., Zou, H., Gu, L., He, Q., 2020. Effects of citrus peel biochar on anaerobic co-digestion of food waste and sewage sludge and its direct interspecies electron transfer pathway study. *Chem. Eng. J.* 398, 125643.
- Jung, M., Ahn, K., Lee, Y., Kim, K., Rhee, J., Park, J.T., Paeng, K., 2001. Adsorption characteristics of phenol and chlorophenols on granular activated carbons (GAC). *Microchem. J.* 70, 123–131.
- Kang, H.J., Lee, S.H., Lim, T.G., Park, H., 2019. Effect of inoculum concentration on methanogenesis by direct interspecies electron transfer: performance and microbial community composition. *Bioresour. Technol.* 291, 121881.
- Kan, T., Strezov, V., Evans, T., 2016. Lignocellulosic biomass pyrolysis: a review of product properties and effects of pyrolysis parameters. *Renew. Sustain. Energy Rev.* 57, 1126–1140.
- Keilueit, M., Nico, P.S., Johnson, M.G., Kleber, M., 2010. Dynamic molecular structure of plant biomass-derived black carbon (biochar). *Environ. Sci. Technol.* 44, 1247–1253.
- Klüpfel, L., Keilueit, M., Kleber, M., Sander, M., 2014. Redox properties of plant biomass-derived black carbon (biochar). *Environ. Sci. Technol.* 48, 5601–5611.
- Kracke, F., Vassilev, I., Kromer, J.O., 2015. Microbial electron transport and energy conservation – the foundation for optimizing bioelectrochemical systems. *Front. Microbiol.* 6, 575.
- Laviron, E., 1979. General expression of the linear potential sweep voltammogram in the case of diffusionless electrochemical systems. *J. Electroanal. Chem.* 101, 19–28.
- Leven, L., Nyberg, K., Schnurer, A., 2012. Conversion of phenols during anaerobic digestion of organic solid waste – a review of important microorganisms and impact of temperature. *J. Environ. Manag.* 95, 99–103.
- Liu, F., Rotaru, A., Shrestha, P.M., Malvankar, N.S., Nevin, K.P., Lovley, D.R., 2012. Promoting direct interspecies electron transfer with activated carbon. *Energy Environ. Sci.* 5, 8982–8989.
- Li, Q., Liu, Y., Yang, X., Zhang, J., Lu, B., Chen, R., 2020. Kinetic and thermodynamic effects of temperature on methanogenic degradation of acetate, propionate, butyrate and valerate. *Chem. Eng. J.* 396, 125366.
- Li, Z., Sellaoui, L., Luiz Dotto, G., Bonilla-Petriciolet, A., Ben Lamine, A., 2019. Understanding the adsorption mechanism of phenol and 2-nitrophenol on a biopolymer-based biochar in single and binary systems via advanced modeling analysis. *Chem. Eng. J.* 371, 1–6.
- Li, Q., Xu, M., Wang, G., Chen, R., Qiao, W., Wang, X., 2018. Biochar assisted thermophilic co-digestion of food waste and waste activated sludge under high feedstock to seed sludge ratio in batch experiment. *Bioresour. Technol.* 249, 1009–1016.
- Lovley, D.R., 2017. Syntrophy goes electric: direct interspecies electron transfer. *Annu. Rev. Microbiol.* 71, 643–664.
- Mao, C., Feng, Y., Wang, X., Ren, G., 2015. Review on research achievements of biogas from anaerobic digestion. *Renew. Sustain. Energy Rev.* 45, 540–555.
- Mohammed, N.A.S., Abuzurayk, R.A., Hamadneh, I., Aldujaili, A.H., 2018. Phenol adsorption on biochar prepared from the pine fruit shells: equilibrium, kinetic and thermodynamics studies. *J. Environ. Manag.* 226, 377–385.
- Poirier, S., Bize, A., Bureau, C., Bouchez, T., Chapleur, O., 2016. Community shifts within anaerobic digestion microbiota facing phenol inhibition: towards early warning microbial indicators? *Water Res.* 100, 296–305.

- Poirier, S., Dejean, S., Chapleur, O., 2018. Support media can steer methanogenesis in the presence of phenol through biotic and abiotic effects. *Water Res.* 140, 24–33.
- Prado, A., Berenguer, R., Esteve-Núñez, A., 2019. Electroactive biochar outperforms highly conductive carbon materials for biodegrading pollutants by enhancing microbial extracellular electron transfer. *Carbon* 146, 597–609.
- Qiu, Y., Hanada, S., Ohashi, A., Harada, H., Kamagata, Y., Sekiguchi, Y., 2008. *Syntrophorhabdus aromaticivorans* gen. nov., sp. nov., the first cultured anaerobe capable of degrading phenol to acetate in obligate syntrophic associations with a hydrogenotrophic methanogen. *Appl. Environ. Microbiol.* 74, 2051–2058.
- Saquin, J.M., Yu, Y.H., Chiu, P.C., 2016. Wood-derived black carbon (biochar) as a microbial electron donor and acceptor. *Environ. Sci. Technol. Lett.* 3, 62–66.
- Siddique, M.N.I., Wahid, Z.A., 2018. Achievements and perspectives of anaerobic co-digestion: a review. *J. Clean. Prod.* 194, 359–371.
- Sun, C., Yu, Q., Zhao, Z., Zhang, Y., 2020. Syntrophic metabolism of phenol in the anodic degradation within a phenol-Cr(VI) coupled microbial electrolysis cell. *Sci. Total Environ.* 723, 137990.
- Thang, P.Q., Jitae, K., Giang, B.L., Viet, N.M., Huong, P.T., 2019. Potential application of chicken manure biochar towards toxic phenol and 2,4-dinitrophenol in wastewaters. *J. Environ. Manag.* 251, 109556.
- Tian, X., Song, Y., Shen, Z., Zhou, Y., Wang, K., Jin, X., Han, Z., Liu, T., 2020. A comprehensive review on toxic petrochemical wastewater pretreatment and advanced treatment. *J. Clean. Prod.* 245, 118692.
- Veeresh, G.S., Kumar, P., Mehrotra, I., 2005. Treatment of phenol and cresols in upflow anaerobic sludge blanket (UASB) process: a review. *Water Res.* 39, 154–170.
- Wang, G., Gao, X., Li, Q., Zhao, H., Liu, Y., Wang, X.C., Chen, R., 2019. Redox-based electron exchange capacity of biowaste-derived biochar accelerates syntrophic phenol oxidation for methanogenesis via direct interspecies electron transfer. *J. Hazard. Mater.*, 121726.
- Wang, G., Li, Q., Li, Y., Xing, Y., Yao, G., Liu, Y., Chen, R., Wang, X.C., 2020. Redox-active biochar facilitates potential electron transfer between syntrophic partners to enhance anaerobic digestion under high organic loading rate. *Bioresour. Technol.* 298, 122524.
- Wu, Y., Wang, S., Liang, D., Li, N., 2020. Conductive materials in anaerobic digestion: from mechanism to application. *Bioresour. Technol.* 298, 122403.
- Xu, Y., Wang, M., Yu, Q., Zhang, Y., 2020. Enhancing methanogenesis from anaerobic digestion of propionate with addition of Fe oxides supported on conductive carbon cloth. *Bioresour. Technol.* 302, 122796.
- Yan, W., Sun, F., Liu, J., Zhou, Y., 2018. Enhanced anaerobic phenol degradation by conductive materials via EPS and microbial community alteration. *Chem. Eng. J.* 352, 1–9.
- Yin, Q., Yang, S., Wang, Z., Xing, L., Wu, G., 2018. Clarifying electron transfer and metagenomic analysis of microbial community in the methane production process with the addition of ferrous oxide. *Chem. Eng. J.* 333, 216–225.
- Yuan, H.-Y., Ding, L.-J., Zama, E.F., Liu, P.-P., Hozzein, W.N., Zhu, Y.-G., 2018. Biochar modulates methanogenesis through electron syntrophy of microorganisms with ethanol as a substrate. *Environ. Sci. Technol.* 52, 12198–12207.
- Yuan, Y., Zhou, S., Xu, N., Zhuang, L., 2011. Electrochemical characterization of anodic biofilms enriched with glucose and acetate in single-chamber microbial fuel cells. *Colloids Surf. B Biointerfaces* 82, 641–646.
- Yu, L., Yuan, Y., Tang, J., Wang, Y., Zhou, S., 2015. Biochar as an electron shuttle for reductive dechlorination of pentachlorophenol by *Geobacter sulfurreducens*. *Sci. Rep.* 5, 16221.
- Zhang, L., Ban, Q., Li, J., 2018a. Microbial community dynamics at high organic loading rates revealed by pyrosequencing during sugar refinery wastewater treatment in a UASB reactor. *Front. Environ. Sci. Eng.* 12, 4.
- Zhang, P., Zheng, S., Liu, J., Wang, B., Liu, F., Feng, Y., 2018b. Surface properties of activated sludge-derived biochar determine the facilitating effects on *Geobacter* co-cultures. *Water Res.* 142, 441–451.
- Zhao, L., Xiao, D., Liu, Y., Xu, H., Nan, H., Li, D., Kan, Y., Cao, X., 2020. Biochar as simultaneous shelter, adsorbent, pH buffer, and substrate of *Pseudomonas citronellolis* to promote biodegradation of high concentrations of phenol in wastewater. *Water Res.* 172, 115494.
- Zhao, Z., Zhang, Y., Yu, Q., Dang, Y., Li, Y., Quan, X., 2016. Communities stimulated with ethanol to perform direct interspecies electron transfer for syntrophic metabolism of propionate and butyrate. *Water Res.* 102, 475–484.